Biochimica et Biophysica Acta 1842 (2014) 1395–1405

Contents lists available at ScienceDirect

Biochimica et Biophysica Acta

journal homepage: www.elsevier.com/locate/bbadis

Apolipoprotein E receptor-2 deficiency enhances macrophage susceptibility to lipid accumulation and cell death to augment atherosclerotic plaque progression and necrosis

Meaghan D. Waltmann [a], Joshua E. Basford [a], Eddy S. Konaniah [a], Neal L. Weintraub [b,1], David Y. Hui [a,*]

[a] Department of Pathology and Laboratory Medicine, University of Cincinnati College of Medicine, Cincinnati, OH USA
[b] Department of Internal Medicine, Division of Cardiovascular Disease, University of Cincinnati College of Medicine, Cincinnati, OH USA

ARTICLE INFO

Article history:
Received 2 November 2013
Received in revised form 2 May 2014
Accepted 7 May 2014
Available online 16 May 2014

Keywords:
Lipoprotein receptor
Atherosclerosis
PPARγ
Apoptosis
p53

ABSTRACT

Genome-wide association studies have linked *LRP8* polymorphisms to premature coronary artery disease and myocardial infarction in humans. However, the mechanisms by which dysfunctions of apolipoprotein E receptor-2 (apoER2), the protein encoded by *LRP8* gene, influence atherosclerosis have not been elucidated completely. The current study focused on the role of apoER2 in macrophages, a cell type that plays an important role in atherosclerosis. Results showed that apoER2-deficient mouse macrophages accumulated more lipids and were more susceptible to oxidized LDL (oxLDL)-induced death compared to control cells. Consistent with these findings, apoER2 deficient macrophages also displayed defective serum-induced Akt activation and higher levels of the pro-apoptotic protein phosphorylated p53. Furthermore, the expression and activation of peroxisome proliferator-activated receptor γ (PPARγ) were increased in apoER2-deficient macrophages. Deficiency of apoER2 in hypercholesterolemic LDL receptor-null mice ($Lrp8^{-/-}Ldlr^{-/-}$ mice) also resulted in accelerated atherosclerosis with more complex lesions and extensive lesion necrosis compared to $Lrp8^{+/+}Ldlr^{-/-}$ mice. The atherosclerotic plaques of $Lrp8^{-/-}Ldlr^{-/-}$ mice displayed significantly higher levels of p53-positive macrophages, indicating that the apoER2-deficient macrophages contribute to the accelerated atherosclerotic lesion necrosis observed in these animals. Taken together, this study indicates that apoER2 in macrophages limits PPARγ expression and protects against oxLDL-induced cell death. Thus, abnormal apoER2 functions in macrophages may at least in part contribute to the premature coronary artery disease and myocardial infarction in humans with *LRP8* polymorphisms. Moreover, the elevated PPARγ expression in apoER2-deficient macrophages suggests that *LRP8* polymorphism may be a genetic modifier of cardiovascular risk with PPARγ therapy.

1. Introduction

Genome-wide linkage studies have shown the association of a single nucleotide polymorphism (SNP) in the *LRP8* gene with the development of familial and premature coronary artery disease (CAD) and myocardial infarction in humans [1,2]. This *LRP8* SNP is also additive with *APOE* genotype, an established genetic risk factor for CVD, in modulating myocardial infarction risk [3]. Four additional *LRP8* SNPs have also been identified as risk factors for familial and premature CAD and myocardial infarction while a haplotype carrying protective alleles from these five *LRP8* SNPs has been shown to confer protection against CAD and myocardial infarction in humans [4]. These studies suggest that apolipoprotein E receptor-2 (apoER2) encoded by the *LRP8* gene may play an important role in atherosclerosis development and progression.

The apolipoprotein E receptor-2 (gene name: LDL receptor-related protein-8, *LRP8*) is a type 1 transmembrane protein structurally similar to other LDL receptor family proteins, with an extracellular domain composed of multiple cysteine-rich ligand binding repeats, a single transmembrane domain and a short cytoplasmic tail that includes several adaptor protein binding motifs. ApoER2 was first identified as a novel LDL receptor family protein expressed predominantly in the brain [5]; hence its role in brain development and its function in maintaining synaptic plasticity and memory are best characterized. In the developmental stage, apoER2 is critical for the ordered formation of cortical layers [6], whereas apoER2 activity is required in the adult brain for long term potentiation as well as maintenance of normal

Abbreviations: ABCA1, ATP binding cassette transporter A1; ApoA-I, apolipoprotein A-I; ApoE, apolipoprotein E; ApoER2, apolipoprotein E receptor-2; CVD, cardiovascular disease; CAD, coronary artery disease; FBS, fetal bovine serum; HDL, high density lipoproteins; LDL, low density lipoproteins; Ldlr, low-density lipoprotein receptor; oxLDL, oxidized low-density lipoproteins; PPARγ, peroxisome proliferator-activated receptor γ; Pcsk9, proprotein convertase subtilisin/kexin type 9; qPCR, quantitative real-time PCR; SNP, single nucleotide polymorphism

* Corresponding author at: Department of Pathology and Laboratory Medicine (ML 0507), University of Cincinnati College of Medicine, 2120 E. Galbraith Road, Cincinnati, OH 45237, USA. Tel.: +1 513 558 9152; fax: +1 513 558 1312.
E-mail address: huidy@ucmail.uc.edu (D.Y. Hui).
[1] Current address: Vascular Biology Center, Georgia Regents University, Augusta, Georgia.

http://dx.doi.org/10.1016/j.bbadis.2014.05.009
0925-4439/

behavior [7]. ApoER2 present in the adult postsynaptic densities of excitatory synapses forms a functional complex with NMDA receptors and is required for normal synaptic neurotransmission and memory [8]. Interestingly, apoER2 is also required for protection against neuronal cell loss during normal aging, but selectively promotes neuronal cell death after injury [9]. These data indicate that apoER2 is required for brain development as well as in the control of neuronal aging and survival after injury in adult brain.

In addition to its predominant expression in the brain, apoER2 is also abundantly expressed in testis where its activity in mediating selenium uptake is critical for male fertility [10,11]. Although expressed at lower levels, apoER2 is also present in cells that participate in atherosclerosis pathogenesis including platelets [12–14], endothelial cells [15–17], and monocytes/macrophages [18,19]. In platelets, apoE binding to apoER2 stimulates nitric oxide synthesis and as a result inhibits agonist-induced platelet activation *in vitro* [14,20]. The platelet apoER2 is also known to modulate adhesion and bleeding time *in vivo* [21]. In endothelial cells, apoE binding to apoER2 also stimulates nitric oxide synthesis and inhibits vascular cell adhesion molecule-1 (VCAM-1) expression [16,22]. However, apoER2 on platelets and endothelial cells also interacts with β2-glycoprotein I–antibody complex [23,24] and mediates leukocyte–endothelial cell adhesion and thrombosis induced by antiphospholipid antibodies through inhibition of endothelial nitric oxide synthase [17].

The functional significance of apoER2 expression in monocytes/macrophages is less clear. In cell culture studies with the U937 human monocytic cells, apoER2 was shown to be one of the receptors in binding activated protein C, leading to activation of the Akt pathway to suppress endotoxin induced procoagulant activity [18]. Additionally, over-expression of apoER2 in RAW 264.7 mouse macrophages has also been reported to increase reelin- and apoE-induced ABCA1 expression and cholesterol efflux, whereas knockdown of apoER2 expression ameliorated the reelin and apoE effects [19]. While these data suggest that apoER2 expression in monocytes/macrophages may benefit atherosclerosis and prevent lipid accumulation, knockdown of apoER2 expression in RAW 264.7 cells had no effect on ABCA1 expression level in the absence of apoE or reelin [19]. Thus, whether apoER2 expression modulates macrophage functions independent of reelin and apoE binding, and its impact on atherosclerosis progression remain unknown. This study was undertaken to address these issues.

2. Materials and methods

2.1. Cell culture

Primary mouse macrophages were isolated from the peritoneum of age-matched *Lrp8*$^{+/+}$ and *Lrp8*$^{-/-}$ mice maintained on a chow diet 4 days after injection of sterile 4% thioglycollate solution into their peritoneal cavities. The isolated cells were allowed to adhere to tissue culture plates for at least 4 h and then washed vigorously with sterile PBS to remove non-adherent cells. The adhering mouse peritoneal macrophages were cultured in RPMI-1640 medium (Thermo Scientific, Florence, KY, USA) containing 10% endotoxin-free fetal bovine serum (FBS, Invitrogen, Grand Island, NY, USA), 100 units/ml penicillin 100 μg/ml streptomycin solution (Thermo Scientific), and 2 mM L-glutamine (Thermo Scientific) at 37 °C and 5% CO_2 unless noted otherwise. Cell counts were performed manually by trypan blue exclusion. The peritoneal macrophages were harvested for further analysis within 4 days of isolation. The mouse macrophage cell line RAW 264.7 cells (ATCC, Manassas, VA, USA) were also cultured under similar conditions. Phosphorylated Akt and total Akt protein levels were assessed in whole cell lysates obtained from RAW 264.7 cells that were seeded at equal densities, allowed to adhere for 16 h overnight, replaced with serum-free media for 24 h, and then returned to fresh media containing 10% FBS for the indicated time.

Table 1
Primer sequences used for quantitative real-time PCR analysis of RNA.

Gene name	Primer sequence
Abca1	Sense 5′-ACCCACCCTACGAACAACATGAGT-3′
	Antisense 5′-AAAGTTTCCAACAACACCGGGAGC-3′
Cd36	Sense 5′-CTGTTATTGGTGCAGTCCTGGC-3′
	Antisense 5′-TATGTGGTGCAGCTGCTACAGC-3′
Gapdh	Sense 5′-GGTGTGAACGGATTTGGCCGTATT-3′
	Antisense 5′-GGTCGTTGATGGCAACAATCTCCA-3′
Lrp1	Sense 5′-CTGAAGGGCTTTGTGGATGAGCATAC-3′
	Antisense 5′-GTAGAAGTTTCCCGTCAGCCAGTC-3′
Lrp8 (apoER2)	Sense 5′-TCATCGTGCCCATAGTGGTAATAG-3′
	Antisense 5′-TTGGTGTTCTTCCGCTTCCAGTTC-3′
Msr1 (SRA)	Sense 5′-TTCAAGGCTGCCCTCATT-3′
	Antisense 5′-AAGCTGAGCTGTTACTATTCCA-3′
Olr1 (Lox1)	Sense 5′-GAAATCCAAAGAGCAGGAGGAG-3′
	Antisense 5′-CTTGTGGACAAGGACCTGAAA-3′
Pparg (PPARγ)	Sense 5′-CTGCAGGCCCTGGAACTG-3′
	Antisense 5′-CGATCTGCCTGAGGTCTGTCA-3′

2.2. Inactivation of Lrp8 gene expression in RAW 264.7 cells

Five lentiviral transduction particles in pLKO.1 vectors expressing shRNA that target the mouse *Lrp8* gene were obtained from Sigma-Aldrich (St. Louis, MO, USA). These lentiviral vectors (identification numbers: TRCN0000176508, TRCN0000177833, TRCN0000178706, TRCN0000176636, TRCN0000177656) were added to RAW 264.7 cells in culture medium containing 8 μg/ml hexadimethrine bromide at a multiplicity of infection of 1 for a total multiplicity of infection of 5.

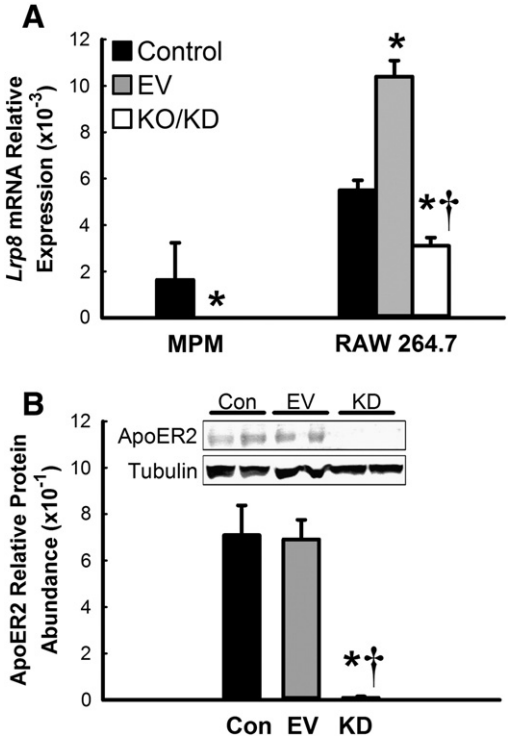

Fig. 1. Generation of Lrp8 deficient macrophages. (A) *Lrp8* mRNA expression levels in peritoneal macrophages (MPM) isolated from *Lrp8*$^{+/+}$ (black bars) and *Lrp8*$^{-/-}$ (white bars) mice, non-transduced control RAW 264.7 cells (black bars), RAW 264.7 cells transduced with an empty vector (gray bars), and RAW 264.7 cells with *Lrp8* knocked down (white bars) normalized to the expression of the housekeeping gene *Gapdh*. (B) Levels of apoER2 protein in non-transduced control RAW 264.7 cells, RAW 264.7 cells transduced with an empty vector (EV), and RAW 264.7 cells with *Lrp8* knocked down (KD) normalized to expression of the tubulin loading control. Inset shows representative immunoblots. MPM $n = 5$ per group, RAW 264.7 mRNA $n = 9$ per group, RAW 264.7 control and knockdown protein $n = 6$ per group, RAW 264.7 empty vector protein $n = 9$. Data represent mean ± SEM, * denotes $P \leq 0.05$ difference from *Lrp8*$^{+/+}$/non-transduced control RAW 264.7 cells, and † denotes $P < 0.05$ difference from empty vector-transfected RAW 264.7 cells.

The lentiviral particles were removed after 16 h and the cells were allowed to recover in fresh culture medium for 24 h. Following puromycin (2–10 μg/ml) selection for 1–2 weeks, the cells were returned to basal medium and were occasionally cultured in the presence of puromycin in order to maintain selection of transduced cells. The transduction was verified based on lack of *Lrp8* mRNA and apoER2 protein as assessed by quantitative real-time PCR and Western blot analysis, respectively. Similarly, RAW 264.7 cells were also transduced with lentiviral particles containing an empty vector (MISSION™ pLKO.1-puro control transduction particles #SHC001V) as a control. All cells were cultured in the absence of puromycin for at least 1 week prior to performing all experiments.

2.3. Quantitative real-time PCR

Total RNA was isolated from mouse peritoneal macrophages and RAW 264.7 cells with the RNeasy® Plus Mini Kit (Qiagen, Valencia, CA, USA) and the RNeasy® Mini Kit (Qiagen), respectively. Genomic DNA was removed by treatment with TURBO DNA-free™ (Ambion, Austin, TX, USA). The RNA was then quantified by measuring the absorbance at 260 nm. The cDNA was synthesized using the iScript™ cDNA Synthesis Kit (Bio-Rad Laboratories, Hercules, CA, USA) and quantitative real-time PCR was performed on an iQ™ 4 iCycler (Bio-Rad) using the iQ™ SYBER® Green Supermix (Bio-Rad) and the sequence specific primers (Table 1). The mRNA expression levels relative to the expression of the *Gapdh* housekeeping gene were calculated using the ΔCT qPCR data analysis method.

2.4. Immunoblot analysis

Whole cell lysates were prepared in RIPA buffer containing 0.05 M Tris-HCl, pH 7.4, 150 mM NaCl, 0.5% sodium deoxycholate, 1% igepal, 0.1% SDS, 1 mM EDTA, 1× phosphatase inhibitor cocktail 2 (Sigma-Aldrich), 1× phosphatase inhibitor cocktail 3 (Sigma-Aldrich), and 1× complete protease inhibitor cocktail (Roche Applied Science, Indianapolis, IN, USA). Nuclear protein extracts were isolated for PPARγ immunoblots from cultured cells using the Nuclear Extraction Kit (Cayman Chemicals, Ann Arbor, MI, USA). The protein concentrations were determined using the Pierce® BCA Protein Assay Kit (Thermo Scientific). Equal amounts of the protein samples were resolved in 10% SDS–polyacrylamide gels in the presence of dithiothreitol (DTT) and were then transferred to Immun-blot PVDF membrane (Bio-Rad). The membranes were blocked with buffer containing 0.1% Tween-20 and 5% nonfat dry milk for 1 h at room temperature. Primary antibody

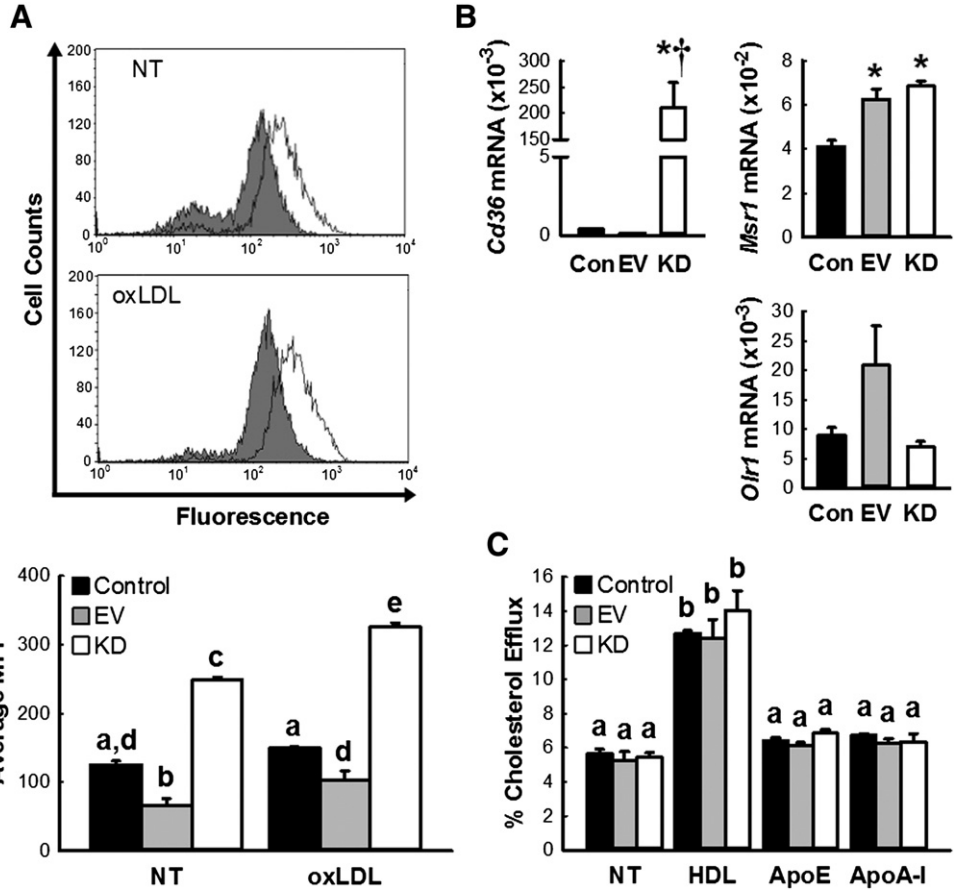

Fig. 2. Neutral lipid accumulation in macrophages lacking apoER2. (A) Non-transduced control RAW 264.7 cells (filled histograms, black bars), RAW 264.7 cells transduced with an empty vector (gray bars), and RAW 264.7 cells with *Lrp8* knocked down (open histograms, KD, white bars) were incubated in the presence or absence (NT) of 50 μg/ml oxLDL overnight. The cells were then analyzed for neutral lipid accumulation by staining with HCS LipidTOX Green Neutral Lipid Stain and subsequent flow cytometry analysis. The median fluorescence intensity (MFI) of the cells was determined by analysis of histograms. Top panels show representative histograms generated by flow cytometry analysis of non-transduced control and knockdown RAW 264.7 cells. RAW 264.7 empty vector $n = 6$, RAW 264.7 non-transduced control and knockdown $n = 3$ per group. Data represent mean ± SEM. Bars with different letters denote $P \leq 0.05$ difference. (B) mRNA levels of *CD36*, *Msr1*, and *Olr1* relative to *Gapdh* in non-transduced control (Con, black bars), empty vector (EV, gray bars), and *Lrp8* shRNA (KD, white bars) transduced RAW264.7 cells. Data represent mean ± SEM from $n = 9$ per group. * denotes $P < 0.05$ difference from non-transduced control cells, and † denotes $P < 0.05$ difference from empty vector transfected RAW 264.7 cells. (C) Non-transduced control RAW264.7 cells (Con, black bars) and RAW264.7 cells transduced with empty vector (EV, gray bars) or *Lrp8* shRNA (KD, white bars) were incubated with [^{3}H]cholesteryl oleate-containing acetylated LDL overnight, followed by incubation in the absence (NT) or presence of HDL, apoE, or apoA-I to facilitate cholesterol efflux. Data are reported as the mean ± SEM percentage of total radioactivity found in the incubation medium from $n = 3$ per group. Bars with different letters denote $P < 0.05$ differences.

incubations were performed overnight at 4 °C and secondary antibody incubations were performed for 1 h at room temperature. The primary antibodies used were anti-Lrp8 (Sigma-Aldrich), anti-phospho-Akt (Serine 473, Cell Signaling Technology, Boston, MA), anti-Akt (Cell Signaling Technology), anti-phospho-p53 (Serine 15, Cell Signaling Technology), anti-p53 (Cell Signaling Technology), anti-PPARγ (Cell Signaling Technology), anti-TATA binding protein (TBP, Cell Signaling Technology), and anti-tubulin (Fisher Scientific, Abcam). The secondary antibodies used were HRP-linked anti-rabbit IgG (Cell Signaling Technology), HRP-linked anti-mouse IgG (Cell Signaling Technology), HRP-linked anti-rat IgG (Sigma-Aldrich), and HRP-linked anti-goat IgG (Dako, Carpinteria, CA). Immunoreactive bands were visualized by chemiluminescence using Pierce® ECL Western Blotting Substrate (Thermo Scientific) and an Amersham™ ECL Advance™ Western Blotting Detection Kit (GE Healthcare, Pittsburgh, PA, USA). Densitometry analysis was performed with digitalized images using ImageJ software (NIH, Bethesda, MD, USA).

2.5. Oxidation of LDL

Preparative ultracentrifugal flotation in KBr solutions between the densities of 1.02 and 1.063 m/ml was used to isolated human LDL from fresh plasma. The isolated LDL was incubated at 37 °C with 12.5 μM $CuSO_4$ overnight and then dialyzed exhaustively against saline solution. The oxidation status of the copper-oxidized LDL was between

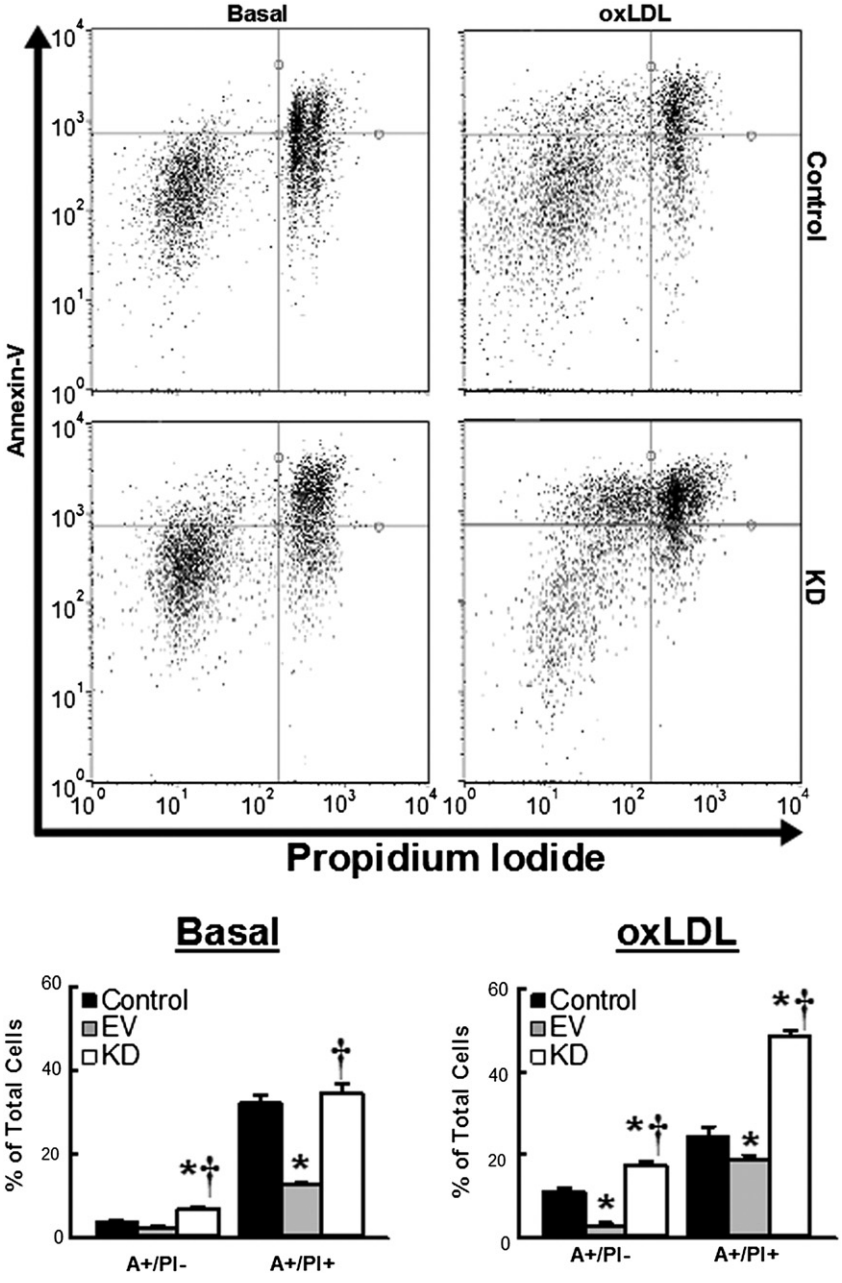

Fig. 3. Oxidized LDL-induced death in control and apoER2 deficient macrophages. Non-transduced control RAW 264.7 cells (black bars), RAW 264.7 cells transduced with an empty vector (gray bars), and RAW 264.7 cells with *Lrp8* knocked down (white bars) were incubated overnight with 500 μg/ml oxLDL. The cells were then stained with APC-conjugated Annexin-V and propidium iodide and analyzed by flow cytometry. Top panels show representative dot plots generated by flow cytometry analysis. Region markers were applied to quantify the percentage of Annexin-V positive pre-apoptotic cells (A+/PI−) and Annexin-V and propidium iodide positive dead cells (A+/PI+) in the populations. The bottom panels show mean ± SEM from $n = 9$ RAW 264.7 empty vector group, and $n = 6$ from RAW 264.7 non-transduced and knockdown groups. * denotes $P < 0.05$ difference from non-transduced control cells, and † denotes $P < 0.05$ difference from empty vector cells.

15 and 17 nmol malonaldehyde per mg of protein as determined by measuring thiobarbituric acid reactive substance (TBARS).

2.6. In vitro neutral lipid accumulation

Cells were seeded at equal densities and incubated overnight in the presence or absence of 50 μg/ml copper-oxidized human LDL. Incubations were performed in media without FBS that contained 5% human lipoprotein deficient serum. Following the overnight incubation, cells were harvested and stained with HCS LipidTOX Green Neutral Lipid Stain (Invitrogen). Flow cytometry analysis was performed using a Guava easyCyte™ 8HT system (Millipore, Billerica, MA, USA) and data were analyzed using Guava InCyte software (Millipore).

2.7. Macrophage cholesterol efflux

The efflux of stored cholesteryl esters from acetylated LDL-challenged macrophages was performed as described previously [25]. Briefly, human LDL was radiolabeled by incubating with cholesterol ester transfer protein and [^{3}H]cholesteryl ester-containing liposomes and then subsequently acetylated in the presence of acetic anhydride and saturated concentrations of sodium acetate. The macrophages were incubated with 50 μg/ml [^{3}H]cholesteryl ester-containing acetylated LDL overnight, equilibrated with serum-free media for 6 h, prior to incubation with 25 μg/ml human HDL, 10 μg/ml apoA-I, or 10 μg/ml recombinant apoE3 for 16 h to induce cholesterol efflux. The amount of [^{3}H]cholesterol transferred to the cholesterol acceptors was determined by measuring the amount of radioactivity in the media. Cellular [^{3}H]cholesterol was quantified in each well following extraction of cellular lipids with hexane:isopropanol (3:2, v:v). The cholesterol efflux results are reported as the radioactivity in the media as a percentage of total radioactivity in each well.

2.8. Flow cytometry analysis of apoptotic cells

Cells were incubated overnight in the presence or absence of 500 μg/ml copper-oxidized human LDL. Following incubation, the cells were gently removed from the plate and Annexin-V and propidium iodide staining was performed using the Annexin-V-APC Apoptosis Detection Kit (eBioscience, San Diego, CA, USA). Flow cytometry analysis was performed using a Guava easyCyte™ 8HT system (Millipore) and data were analyzed using Guava InCyte software (Millipore). In selected experiments, CD36 blockage was achieved using the mouse monoclonal anti-CD36 IgG (clone FA6.152, Beckman Coulter) as described previously [26]. Macrophages were pre-incubated with the anti-CD36 IgG or a mouse monoclonal IgG1 isotype control (Cell Signaling) for 1 h prior to the addition of copper-oxidized LDL.

2.9. Transient knockdown of PPARγ in RAW264.7 cells

RAW 264.7 cells were transiently transfected with Silencer Select small interfering RNA (siRNA) specifically targeting mouse PPARγ (gene name: *Pparg*) or the non-targeting negative ctornol No. 2 siRNA (Life Technologies). The sequences of the *Pparg* targeting siRNA are: sense 5′-GGGCGAUCUUGACAGGAAtt-3′ and antisense 5′-UUUCCUGU CAAGAUCGCCCte-3′. The siRNA was transfected into the cells by Nucleofector™ using Amaxa Cell Line Nucleofector™ Kit V (Lonza) according to the manufacturer's instructions. Following transfection, cells were incubated in RPMI-1640 medium (Thermo Scientific) containing 10% endotoxin-free FBS, 100 units/ml penicillin–100 μg/ml streptomycin solution (Thermo Scientific), and 2 mM L-glutamine at 37 °C and 5% CO_2 for 48 h prior to analysis.

2.10. Atherosclerotic lesion analysis

The *Lrp8*$^{-/-}$ mice were previously generated in a mixed genetic background of C57BL/6 and 129sv (16). The *Lrp8*$^{-/-}$ mice were backcrossed with C57BL/6J (Jackson Laboratories) mice for 10 generations to produce *Lrp8*$^{-/-}$ mice on a congenic C57BL/6 background. Female *Lrp8*$^{-/-}$ mice on a congenic C57BL/6 background were also bred with male *Ldlr*$^{-/-}$ mice on the same background (Jackson laboratories) to obtain *Lrp8*$^{+/-}$ *Ldlr*$^{+/-}$ offsprings, which were then mated to obtain *Lrp8*$^{+/+}$*Ldlr*$^{-/-}$ and *Lrp8*$^{-/-}$*Ldlr*$^{-/-}$ littermates. Age-matched male mice on congenic C57BL/6 background were used for all experiments. Mice were fed a standard rodent chow diet and were maintained in a specific pathogen-free environment on a 12 h light/dark cycle. For atherosclerosis studies, mice were fed a high fat (21.2% by weight, 42% kcal) and high cholesterol (0.15% by weight) Western-type diet (TD88137; Harlan Teklad, Madison, WI, USA) for 24 weeks. All procedures and animal care was approved by the University of Cincinnati Institutional Animal Care and Use Committee.

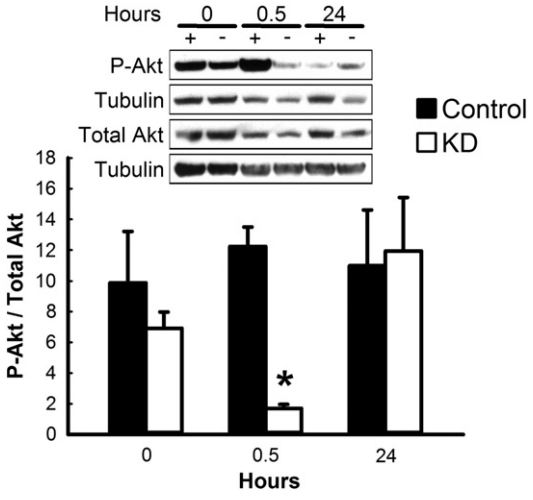

Fig. 4. Activated Akt protein levels in control and apoER2 deficient macrophages. Immunoblots of protein extracts from non-transduced control RAW 264.7 (black bars, +) and *Lrp8* knockdown RAW 264.7 cells (white bars, −). Following serum starvation, cells were incubated with fresh media containing 10% FBS for 0, 0.5, and 24 h. Analysis of Akt activation was performed using antibodies targeting Akt phosphorylated at serine 473 (P-Akt). Data are normalized to the tubulin loading control. Inset shows representative immunoblots and the mean ± SEM from $n = 8$ or 9 is shown in the graph. * denotes $P < 0.05$ difference from non-transduced control cells.

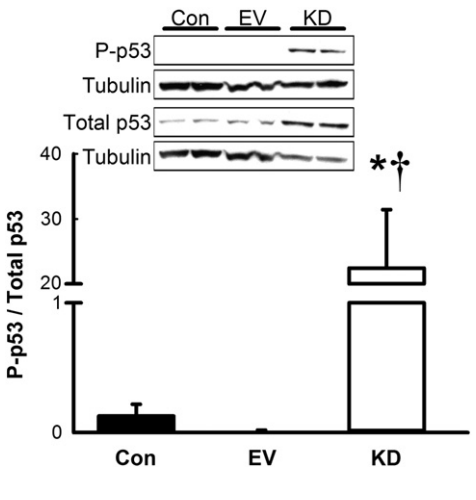

Fig. 5. Phosphorylation of p53 in control and apoER2-deficient macrophages. Immunoblots of protein extracts from non-transduced control (Con, black bar) RAW264.7 cells or RAW264.7 cells transduced with an empty vector (EV, gray bar) or *Lrp8* shRNA (KD, white bar) after 24 h incubation in standard culture medium. Analysis of p53 was performed using antibodies against serine-15 phosphorylated p53 and total p53 and normalized to tubulin loading control. Inset shows representative immunoblots and the data represent mean ± SEM from $n = 9$ (EV group) or $n = 6$ (Control and KD groups) experiments. * and † denote $P < 0.05$ differences from non-transduced and empty vector-transduced RAW 264.7 cells, respectively.

Atherosclerotic lesions in mice were assessed according to the procedure as previously described [27,28]. Briefly, mice were anesthetized and perfused with PBS for 5 min followed by a 5 min perfusion with 4% paraformaldehyde. Following dissection, the upper half of the heart and the proximal aorta were stored in 4% paraformaldehyde for 2 days. Tissues were cryopreserved in 30% sucrose at 4 °C for 2 days prior to being embedded in OCT compound for frozen section preparation. Cryosections of 5-μm thickness through the aortic valve region of the aortic root were stained with Oil Red O to measure neutral lipid accumulation. Serial sections were also stained with Sirius Red to identify collagen deposition. The necrotic core area was measured as the hematoxylin and eosin-negative regions in the intima. TUNEL staining was performed according to manufacturer's instruction with the In Situ Cell Death Detection Kit (Roche) containing fluorescein-conjugated dUTPs. The p53 and PPARγ antigens were detected in aortic sections by immunofluorescent staining with anti-p53 (Cell Signaling Technology) and anti-PPARγ (Abcam, Cambridge, MA, USA) primary antibodies followed by secondary antibodies conjugated to Alexa594 (Invitrogen). The CD68 antigen was detected in the double stained sections with anti-CD68 (Abcam) and anti-rat secondary antibodies conjugated to Alexa488. All of the immunofluorescence sections and the TUNEL-stained sections were counterstained with 4,6-diamidino-2-phenylindole (DAPI). Images were obtained with an Olympus BX61 microscope and quantitative analysis of lesion areas in digitalized images was performed using ImageJ software (NIH).

2.11. Plasma cholesterol measurements

Blood was collected from mice via tail bleed in EDTA-coated Microvette® CB 300 capillary tubes (Sarstedt) after a 16 h overnight fast. Following separation by centrifugation, the plasma was removed and cholesterol levels were measured using Infinity™ Total Cholesterol Reagent (Thermo-Scientific).

2.12. Statistical analysis

Statistical analysis was performed using SigmaPlot (SysStat Software, San Jose, CA, USA). Values were expressed as mean ± standard error (SEM). A two-tailed Student's *t*-test was used when paired comparisons were made. A one-way ANOVA with Holm–Sidak post-hoc analysis was used when multiple comparisons were made. Statistical significance was determined as differences with $P \leq 0.05$.

3. Results

3.1. Generation of ApoER2 deficient mouse macrophages

Quantitative real-time PCR (qPCR) analysis of cellular RNA isolated from peritoneal macrophages of C57BL/6 mice confirmed the expression of apoER2 in macrophages (Fig. 1A). The specificity of the qPCR reaction was verified by the lack of detectable qPCR product when

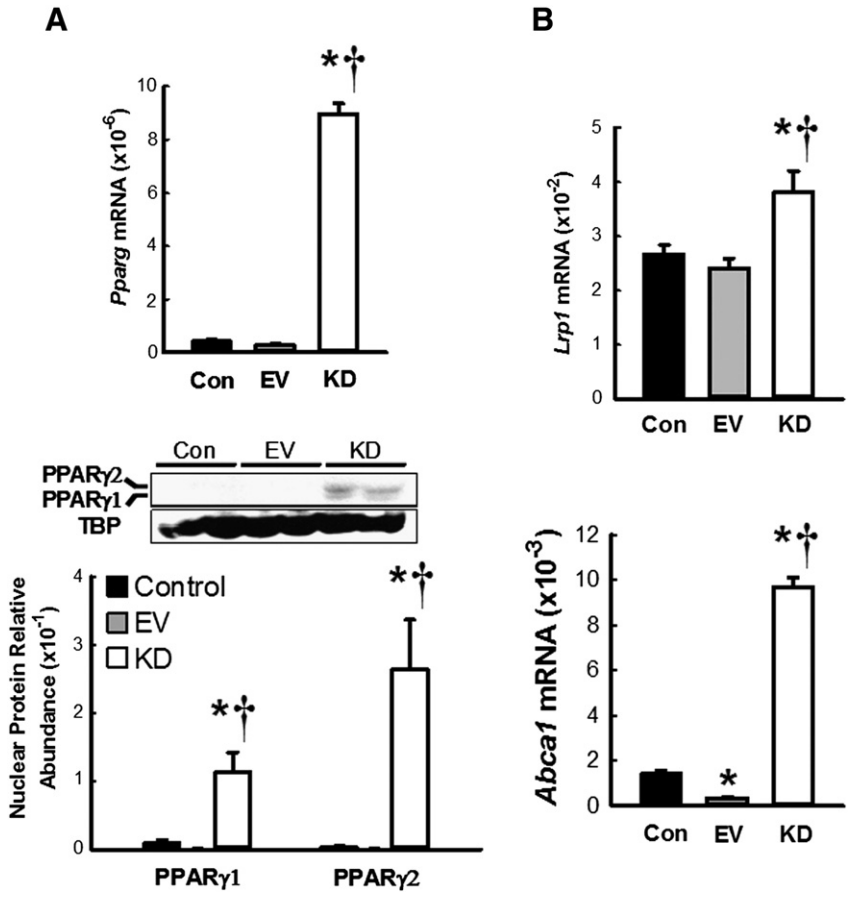

Fig. 6. PPARγ expression and activation in control and apoER2 deficient macrophages. (A) The *Pparg* (PPARγ) mRNA and nuclear PPARγ1/2 protein levels in non-transduced control (black bars), empty vector (gray bars), and *Lrp8* knockdown (white bars) RAW 264.7 cells after 24 h incubation in standard culture conditions. Data were normalized to *Gapdh* mRNA and TATA-binding protein (TBP), respectively. Inset shows representative immunoblots of nuclear proteins from RAW 264.7 cells. (B) mRNA levels of the PPARγ-responsive genes *Lrp1* and *Abca1* relative to *Gapdh* in non-transduced control (black bars), empty vector (gray bars), and *Lrp8* shRNA transduced (open bars) RAW 264.7 cells. mRNA $n = 9$ per group, RAW 264.7 empty vector protein $n = 9$, RAW 264.7 non-transduced control and knockdown protein $n = 6$. Data represent mean ± SEM. * denotes $P < 0.05$ difference from non-transduced control, and † denotes $P < 0.05$ difference from empty vector cells.

RNA isolated from peritoneal macrophages of the apoER2-defective *Lrp8*$^{-/-}$ mice was used as template (Fig. 1A). Interestingly, the *Lrp8*$^{-/-}$ peritoneal macrophages displayed dramatically reduced viability *in vitro* which reached as low as a 65% reduction in the number of viable *Lrp8*$^{-/-}$ cells compared to *Lrp8*$^{+/+}$ cells after 3 days in culture. The difficulty in maintaining apoER2-defective peritoneal macrophages in culture precluded their use to assess the role of apoER2 in macrophage functions. Fortunately, apoER2 was found to be present in mouse RAW 264.7 macrophages and its knockdown with shRNA led to a significant decrease in both *Lrp8* mRNA (Fig. 1A) and apoER2 protein levels (Fig. 1B) while maintaining cell viability in culture.

3.2. ApoER2 deficient macrophages accumulate more intracellular lipids and are more susceptible to oxidized LDL-induced cell death

One function of macrophages is the scavenging of lipids, particularly those derived from oxLDL, during atherogenesis. Therefore, we set out to determine the impact of apoER2 deficiency on neutral lipid accumulation in RAW 264.7 macrophages. The apoER2-deficient RAW 264.7 macrophages showed more neutral lipid accumulation compared to control RAW 264.7 cells under basal conditions (Fig. 2A). Importantly, the apoER2-deficient RAW 267.4 cells also accumulated more neutral lipids following treatment with oxidized LDL (oxLDL) (Fig. 2A). The uptake of oxLDL by macrophages is regulated by scavenger receptors. Interestingly, we observed higher CD36 mRNA level in the apoER2-deficient macrophages, but no difference in Lox (gene name: *Olr1*) mRNA (Fig. 2B). A significant higher level of mRNA for scavenger receptor A (gene name: *Msr1*) was also observed in the apoER2-deficient macrophages compared to the non-transduced control cells, but a similar increase was observed in macrophages transduced with the empty vector, suggesting that the *Msr1* mRNA increase was a result of viral vector transduction. Furthermore, we did not observe any alterations in the ability of apoER2-deficient macrophages to efflux cholesterol to HDL, apoA-I or apoE (Fig. 2C). Taken together, these data suggest that the apoER2-deficient macrophages accumulate more neutral lipids due to increased uptake of exogenous lipids.

In addition to causing lipid accumulation, oxLDL also promotes macrophage cell death [29,30]. Therefore, we also compared the susceptibility of control and apoER2-deficient RAW 264.7 macrophages to oxLDL-induced cell death. The macrophages were incubated overnight in the presence or absence of oxLDL and cell death was assessed by flow cytometry based on the percentage of cells with positive Annexin-V and propidium iodide (PI) staining. Results showed a significant increase in the percentage of dead cells in the apoER2-deficient cell population compared to the control cells following overnight incubation with oxLDL (Fig. 3). Moreover, while there was no significant difference in the percentage of dead cells (Annexin-V+, PI+) between control and apoER2-deficient cells when cultured under basal conditions without oxLDL treatment (Fig. 3), an increase in the percentage of apoER2-deficient cells undergoing early apoptosis (Annexin-V+, PI−) compared to control cells was observed in the presence or absence of oxLDL. Thus, the defective apoER2 expression in macrophages induced cell stress and enhanced their susceptibility to oxLDL-induced cell death.

3.3. ApoER2 deficiency promotes pro-apoptotic cell signaling in macrophages

The next series of experiments examined the mechanism by which apoER2 deficiency enhances the susceptibility of macrophages to oxLDL-induced cell death. In these experiments, we compared the expression and activation of apoptosis-related proteins in control and apoER2-deficient RAW 264.7 macrophages. Immunoblotting performed with whole cell lysates from these cells showed that serum-induced activation of the pro-survival protein Akt was reduced significantly in the *Lrp8*-inactivated cells compared to control cells following a 30 min incubation period (Fig. 4). Additionally, a significantly higher level of p53 phosphorylation was also detected in the apoER2-deficient cells compared to control cells (Fig. 5).

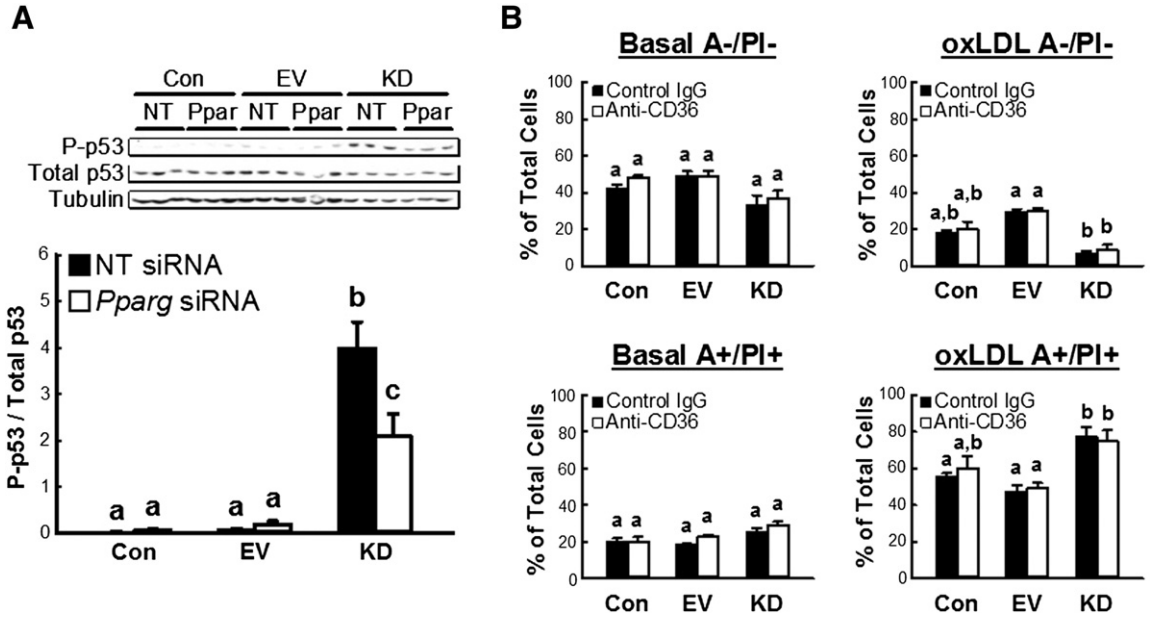

Fig. 7. Effects of PPARγ and CD36 inhibition on macrophage viability. (A) Non-transduced RAW264.7 cells (Con) and cells transduced with empty vector (EV) or *Lrp8*shRNA (KD) were transiently transfected with non-targeting control siRNA (NT, black bars) or siRNA targeting PPARγ (white bars). Analysis of p53 levels and phosphorylation was performed using antibodies against total or serine-15 phosphorylated forms of p53. Data are normalized to tubulin loading control prior to normalization of phosphorylated p53 to total p53. Inset shows representative immunoblots. (B) The RAW264.7 cells were incubated with 20 μg/ml anti-CD36 (white bars) or isotype control IgG (black bars) for 1 h prior to overnight incubation with 250 μg/ml oxLDL. The cells were stained with APC-conjugated Annexin-V and propidium iodide for flow cytometry analysis. The percentage of viable and dead cells was calculated as a percentage of cells that were negative or positive for Annexin-V and propidium iodide staining, respectively. The data are reported as mean ± SEM from $n = 3$ per group and different letters in the bars denote $P < 0.05$ differences.

3.4. Macrophage PPARγ expression and activation are increased in the absence of ApoER2

One mechanism that leads to p53 phosphorylation and stabilization is through activation of the nuclear receptor peroxisome proliferator-activated receptor γ (PPARγ) [31-36]. Analysis of PPARγ mRNA levels by qPCR showed elevated PPARγ-encoding *Pparg* mRNA expression in apoER2-deficient RAW 264.7 cells compared to control cells (Fig. 6A). Western blot analysis of nuclear extracts from these cells revealed an 82-fold increase of PPARγ2 and a 13-fold increase of PPARγ1 in the nucleus of apoER2-deficient macrophages (Fig. 6A). The increased presence of PPARγ-1/2 in the nucleus of apoER2-deficient RAW 264.7 macrophages also resulted in elevated mRNA levels of PPARγ-responsive genes such as *Cd36*, *Lrp1*, and *Abca1* in comparison to the levels observed in control cells (Figs. 2B and 6B). Taken together, these results suggested that the aberrant up-regulation of PPARγ expression may be responsible for the increased susceptibility of apoER2-deficient macrophages to stimulant-induced cell death.

3.5. Inhibition of PPARγ, but not CD36, partially rescues the ApoER2-deficient macrophage phenotype

The relationship between elevated PPARγ expression with the sensitivity of the apoER2-deficient macrophage to cell death was assessed by transient knockdown of PPARγ in the macrophages with siRNA. The knockdown of PPARγ resulted in a significant reduction in the phosphorylation of p53 in the apoER2-deficient macrophages compared to cells transfected with control siRNA (Fig. 7A). Since the PPARγ-responsive gene CD36 was up-regulated in the apoER2-deficient macrophages, which likely resulted in the increased neutral lipid accumulation observed in these cells, we also determined if inhibiting CD36-mediated oxLDL uptake also desensitized the apoER2-deficient macrophages to oxLDL-induced cell death. Interestingly, we found that pre-treatment of the macrophages with a CD36 blocking antibody did not have any effect on the number of viable (Annexin-V−, PI−) or dead (Annexin-V+, PI+) macrophages in the presence or absence of oxLDL (Fig. 7B). Taken together, these data suggest that the increased sensitivity of apoER2-deficeint macrophages to oxLDL-induced cell death is due to elevated PPARγ expression and its induction of p53 phosphorylation, and that this mechanism is independent of PPARγ-induced CD36 expression.

3.6. Inactivation of Lrp8 in hypercholesterolemic mice enhances atherosclerotic plaque complexity and necrosis

The physiological significance of increased oxLDL-induced lipid accumulation and cell death of $Lrp8^{-/-}$ macrophages toward atherosclerosis was queried by analyzing the composition of atherosclerotic plaques in hypercholesterolemic $Ldlr^{-/-}$ mice with or without *Lrp8* gene deletion. For these experiments, $Lrp8^{+/+}Ldlr^{-/-}$ and $Lrp8^{-/-}$ $Ldlr^{-/-}$ mice were fed a Western type diet for 24 weeks. Marked hypercholesterolemia occurred in all $Ldlr^{-/-}$ mice, but no difference in plasma cholesterol levels was observed between $Lrp8^{+/+}Ldlr^{-/-}$ and $Lrp8^{-/-}Ldlr^{-/-}$ mice (1,617 ± 94 vs. 1,672 ± 61 mg/dl, $n = 10$).

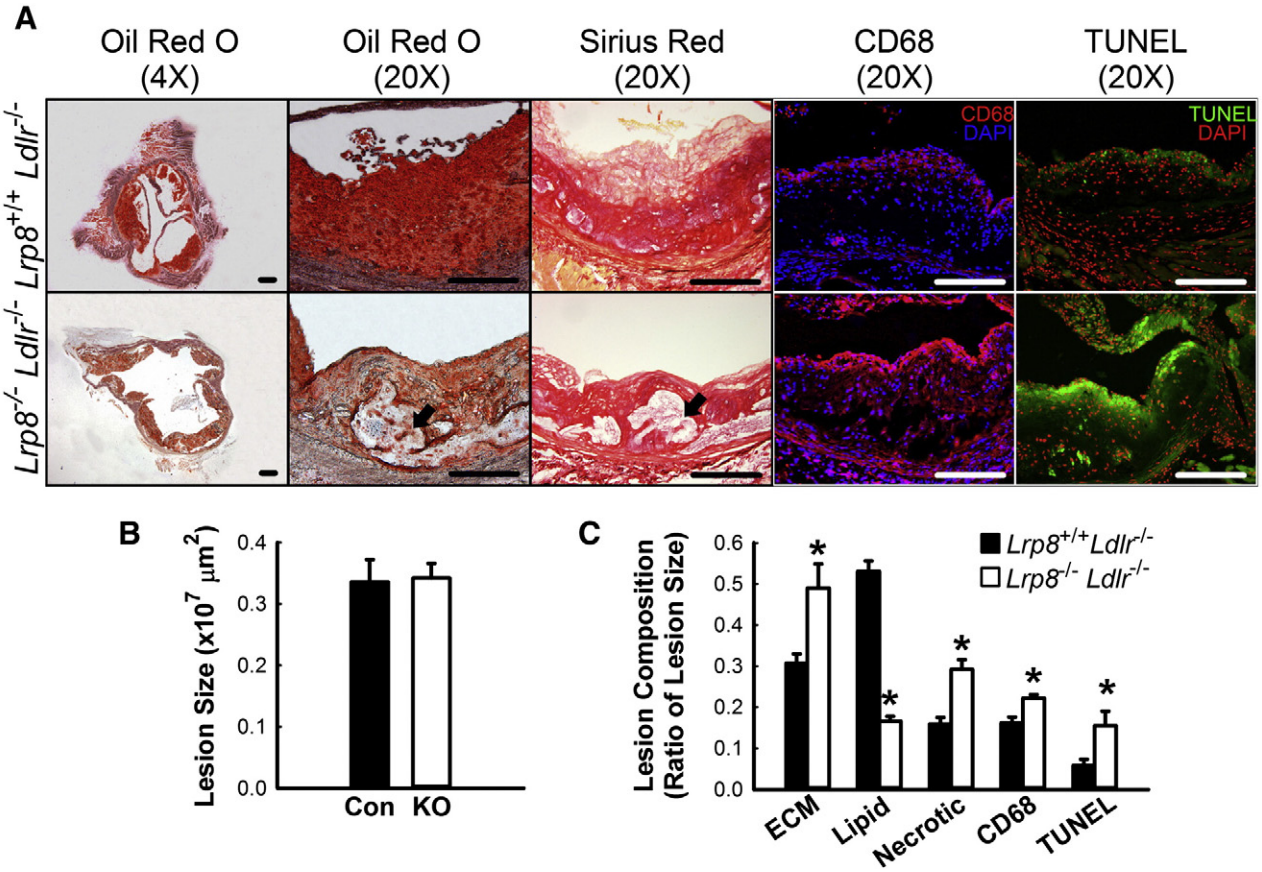

Fig. 8. Atherosclerotic lesion development in $Ldlr^{-/-}$ mice with or without apoER2 expression. Age-matched male $Lrp8^{+/+}{}^{L}dlr^{-/-}$ (Con, black bars), and $Lrp8^{-/-}$ $Ldlr^{-/-}$ (KO, white bars) mice were fed a high fat and high cholesterol Western-type diet for 24 weeks. (A) Representative photomicrographs of aortic root lesions from $Lrp8^{+/+}{}^{L}dlr^{-/-}$ and $Lrp8^{-/-}$ $Ldlr^{-/-}$ mice stained with Oil Red O or Sirius Red, or labeled with fluorescent antibodies against CD68 (red, DAPI counterstain is blue) or fluorescent TUNEL (green, DAPI counterstain is red). The scale bars represent 100 μm. (B) Morphometric analysis of the aortic root atherosclerotic lesion sizes. (C) Morphometric analysis of extracellular matrix area (ECM), lipid-rich area (lipid), and necrotic core area (necrotic) in the aortic root lesions of mice following 24 weeks on a Western diet. Data are expressed as ratios of compositional area to total lesion size. Lesion size $n = 6$, ECM $n = 4$, lipid $n = 7$, necrotic $n = 7$, TUNEL $n = 3$–4, and CD68, $n = 4$ per group. Mean ± SEM. * denotes $P \leq 0.05$ difference from $Lrp8^{+/+}Ldlr^{-/-}$ mice.

Cross-sectional analysis of the atherosclerotic lesions in the aortic roots of these animals also showed similar lesion sizes between $Lrp8^{+/+}Ldlr^{-/-}$ and $Lrp8^{-/-}Ldlr^{-/-}$ mice (Fig. 8). Interestingly, extensive necrosis was detected in the lesions of $Lrp8^{-/-}Ldlr^{-/-}$ mice whereas minimal necrosis was detected in $Lrp8^{+/+}Ldlr^{-/-}$ mice. Additionally, increased TUNEL-positive area that colocalized with CD68-positive staining was detected in the lesions of $Lrp8^{-/-}Ldlr^{-/-}$ mice compared to that observed in $Lrp8^{+/+}Ldlr^{-/-}$ mice. Morphometric quantification of the lesions revealed that the $Lrp8^{-/-}Ldlr^{-/-}$ lesions contained significantly more extracellular matrix components, necrotic materials, and TUNEL-positive macrophages, but less lipid-rich area (Fig. 8).

The characteristics responsible for the increased necrosis in lesion areas of $Lrp8^{-/-}Ldlr^{-/-}$ mice were further examined by immunofluorescence microscopy. Significantly more p53 positive immunofluorescence was observed near the edges of the expanding atherosclerotic plaque in $Lrp8^{-/-}Ldlr^{-/-}$ mice compared to that in $Lrp8^{+/+}Ldlr^{-/-}$ mice (Fig. 9A). These p53-positive cells co-localized with CD68-positive macrophages (Fig. 9A). The CD68-positive macrophages near the edges of the expanding plaque of $Lrp8^{-/-}Ldlr^{-/-}$ mice also showed increased PPARγ-positive macrophages compared to that observed in $Lrp8^{+/+}Ldlr^{-/-}$ mice (Fig. 9B). Since previous studies have shown that sustained macrophage apoptosis occurring at the edge of the atherosclerotic lesions contributes to plaque necrosis, with the necrotic core resulting from gradual apoptotic cell accumulation that becomes secondarily necrotic [37], these observations are consistent with our *in vitro* observations of increased apoER2-defective macrophages with elevated expression of PPARγ and p53 may be responsible for the elevated necrosis observed in atherosclerotic lesions of $Lrp8^{-/-}Ldlr^{-/-}$ mice.

4. Discussion

The current study showed that *Lrp8* gene inactivation in mice has no impact on plasma cholesterol levels, but influences atherosclerosis by regulating functions of cells involved with atherosclerosis. Previous studies have indicated that apoER2 expressed in platelets and endothelial cells modulates leukocyte–endothelial cell adhesion, nitric oxide synthesis, and thrombosis. The current study showed that apoER2 expression in macrophages also modulates atherosclerosis by limiting oxLDL-induced lipid accumulation and cell death. Indeed, hypercholesterolemic $Ldlr^{-/-}$ mice with defective apoER2 displayed advanced atherosclerotic lesions with necrotic cores. The co-localization of the apoptotic markers TUNEL and p53 with the macrophage marker CD68 in the atherosclerotic plaques of $Lrp8^{-/-}Ldlr^{-/-}$ mice is consistent with the interpretation that the advanced necrotic plaque is derived from macrophage cell death.

The role of apoER2 in preserving cell viability has been documented previously in several cell types under both *in vitro* and *in vivo* conditions. For example, apoER2 has been shown to control neuronal survival in adult brain and its inactivation results in accelerated age-dependent

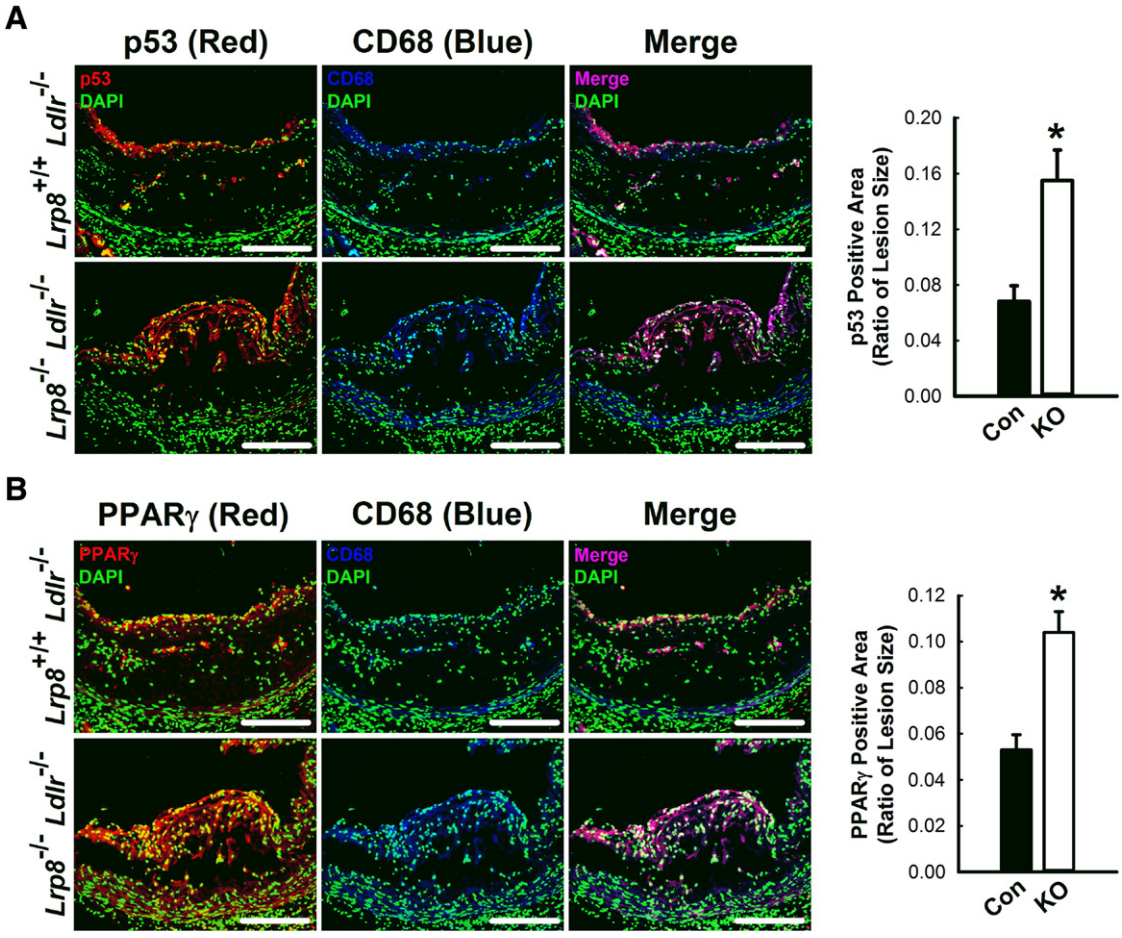

Fig. 9. Immunofluorescent staining of p53- and PPARγ-macrophages in $Ldlr^{-/-}$ mice with or without apoER2 expression after 24 weeks on Western diet. Representative photomicrographs and morphometric analyses of aortic root lesions from $Lrp8^{+/+L}dlr^{-/-}$ (Con, black bars) and $Lrp8^{-/-}$ $Ldlr^{-/-}$ (KO, white bars) mice with immunofluorescent antibodies against (A) p53 (red) or (B) PPARγ. The sections were co-stained with CD68 antibodies (blue), and counterstained with DAPI (green). Morphometric analyses of p53-positive and PPARγ-positive areas in the aortic root lesions expressed as ratios of positively-stained area to total lesion size. The scale bars represent 100 μm. $n = 6$ per group. Mean ± SEM. * denotes $P < 0.05$ difference from $Lrp8^{+/+L}dlr^{-/-}$ mice.

neuronal cell death [9]. The neuroprotective properties of apoER2 were also demonstrated by studies showing that reduced *Lrp8* mRNA abundance associated with increased neurodegeneration in mice with Niemann–Pick type C 1 gene inactivation when compared to wild type controls [38], and the knockdown of *Lrp8* in primary neurons reversed the anti-apoptotic effect of proprotein convertase subtilisin/kexin type 9 (Pcsk9) deficiency [39]. Interestingly, Pcsk9 has also been shown to regulate apoptosis in apoER2-expressing human umbilical vein endothelial cells suggesting that apoER2 may have a similar function in vascular cells [40]. The mechanism underlying the cytoprotective properties of apoER2 appears to be related to its cell signaling properties including ligand binding-induced phosphorylation of the adaptor protein Dab-1 with subsequent activation of Akt [18,41]. In the current study, we showed that apoER2 deficiency in macrophages also resulted in defective Akt activation, up-regulation of pro-apoptotic protein p53 phosphorylation, and enhanced susceptibility of the macrophages to stress-induced death *in vitro* and *in vivo*. Taken together, these data suggest that apoER2 has a pro-survival function in macrophages and protects against oxLDL-induced apoptosis via activation of the pro-survival protein Akt.

Macrophage apoptosis and cell death due to defective Akt activation with p53 and cathepsin L accumulation are also PPARγ-regulated processes [33,35,36]. Indeed, elevated nuclear PPARγ levels and mRNA expression were observed in apoER2-deficient macrophages. The apoER2-deficient macrophages also exhibited robust expression of *Cd36*, another PPARγ-responsive gene that is known to promote atherosclerosis [42,43]. Thus, apoER2 deficiency-induced PPARγ activation in macrophages results in enhanced oxLDL-induced cytotoxicity which likely promotes the formation of more advanced atherosclerotic lesions. However, it is important to note that PPARγ activation in macrophages has been reported to have anti-atherosclerosis properties including the suppression of C–C chemokine receptor-2 expression and activation of cholesterol efflux [44,45]. In fact, the activation of PPARγ by pharmacological agents or macrophage-specific *Mal1* gene deletion has also been shown to reduce atherosclerosis in $Ldlr^{-/-}$ mice [46,47]. The apparent discrepancy may be due to the time when atherosclerotic lesions were assessed and the methodology used to assess atherosclerosis advancement. The earlier studies examined atherosclerosis after feeding the Western type diet for 10 to 14 weeks, and atherosclerosis progression was determined based on lesion size at the aortic roots without detailed characterization of lesion composition. In order to examine the advanced stages of atherosclerosis it is likely necessary for mice to be maintained on a Western type diet for longer than 10 to 14 weeks. Therefore, we assessed lesion composition after 24 weeks on Western diet and showed that apoER2 deletion promotes atherosclerotic plaque necrosis and PPARγ co-localizes with CD68-positive macrophages in the edges of the expanding plaque where apoptosis occurs. Taken together, this suggests that PPARγ induction may have a biphasic influence in atherosclerosis progression with the potentially beneficial effects at earlier time points offset by the detrimental effects on lesion necrosis at later phases of atherosclerosis. This interpretation is consistent with reports showing similar biphasic effects of the PPARγ agonist pioglitazone on atherosclerosis in $Ldlr^{-/-}$ mice [48].

In summary, this study has focused on the role of apoER2 in modulating macrophage functions and viability. Our data showed that apoER2 expression in macrophages reduces stress-induced cell death which may potentially retard the development of advanced atherosclerotic plaques *in vivo*. Additionally, it is important to note that ligand ligation of apoER2 may also reduce atherosclerosis by suppressing the inflammatory functions of macrophages. This possibility, along with the mechanism underlying apoER2 modulation of PPARγ activation, is under investigation. Regardless, the observation of sustained PPARγ activation leading to enhanced lipid accumulation in macrophages and reducing macrophage viability points to another mechanism contributing to the potential adverse effects of PPARγ agonists on cardiovascular diseases [49–51]. Importantly, our data also suggest that *LRP8* gene polymorphism may be a genetic modifier in determining the risk of cardiovascular events associated with PPARγ agonist therapy.

Acknowledgement

This study was supported by the U.S. National Institutes of Health grants DK74932 and HL118001 (to D.Y.H.). M.D.W. was a pre-doctoral fellow in the U.S. National Institutes of Health training grant T32 HL007382.

References

[1] G.-Q. Shen, L. Li, D. Girelli, S.B. Seidelmann, S. Rao, C. Fan, J.E. Park, Q. Xi, J. Li, Y. Hu, O. Olivieri, K. Marchant, J. Barnard, R. Corrocher, R.C. Elston, J. Cassano, S. Henderson, S. L. Hazen, E.F. Plow, E.J. Topol, Q.K. Wang, An LRP8 variant is associated with familial and premature coronary artery disease and myocardial infarction, Am. J. Hum. Genet. 81 (2007) 780–791.
[2] Q. Wang, S. Rao, G.-Q. Shen, L. Li, D.J. Moliterno, L.K. Newby, W.J. Rogers, R. Cannata, E. Zirzow, R.C. Elston, E.J. Topol, Premature myocardial infarction novel susceptibility locus on chromosome 1P34-36 identified by genomewide linkage analysis, Am. J. Hum. Genet. 74 (2004) 262–271.
[3] N. Martinelli, O. Olivieri, G.-Q. Shen, E. Trabetti, F. Pizzolo, F. Busti, S. Friso, A. Bassi, L. Li, Y. Hu, P. Pignatti, R. Corrocher, Q. Wang, D. Girelli, Additive effect of LRP8/APOER2 R952Q variant to APOE epsilon2/epsilon3/epsilon4 genotype in modulating apolipoprotein E concentration and the risk of myocardial infarction: a case-control study, BMC Med. Genet. 10 (2009) 41.
[4] G.-Q. Shen, D. Girelli, L. Li, O. Olivieri, N. Martinelli, Q. Chen, E.J. Topol, Q.K. Wang, Multi-allelic haplotype association identifies novel information different from single-SNP analysis: a new protective haplotype in the LRP8 gene is against familial and early-onset CAD and MI, Gene 521 (2013) 78–81.
[5] D.H. Kim, H. Iijima, K. Goto, J. Sakai, H. Ishii, H.J. Kim, H. Suzuki, H. Kondo, S. Saeki, T. Yamamoto, Human apolipoprotein E receptor 2. A novel lipoprotein receptor of the low density lipoprotein receptor family predominantly expressed in brain, J. Biol. Chem. 271 (1996) 8373–8380.
[6] M. Trommsdorff, M. Gotthardt, T. Hiesberger, J. Shelton, W. Stockinger, J. Nimpf, R.E. Hammer, J.A. Richardson, J. Herz, Reeler/disabled-like disruption of neuronal migration in knockout mice lacking the VLDL receptor and apoE receptor 2, Cell 97 (1999) 689–701.
[7] U. Beffert, A. Durudas, E.J. Weeber, P.C. Stolt, K.M. Giehl, J.D. Sweatt, R.E. Hammer, J. Herz, Functional dissection of reelin signaling by site-directed disruption of disabled-1 adaptor binding to apolipoprotein E receptor 2: distinct roles in development and synaptic plasticity, J. Neurosci. 26 (2006) 2041–2052.
[8] U. Beffert, E.J. Weeber, A. Durudas, S. Qiu, I. Masiulis, J.D. Sweatt, W.-P. Li, G. Adelmann, M. Frotscher, R.E. Hammer, J. Herz, Modulation of synaptic plasticity and memory by reelin involves differential splicing of the lipoprotein receptor ApoER2, Neuron 47 (2005) 567–579.
[9] U. Beffert, F.N. Farsian, I. Masiulis, R.E. Hammer, S.O. Yoon, K.M. Giehl, J. Herz, ApoE receptor 2 controls neuronal survival in the adult brain, Curr. Biol. 16 (2006) 2446–2452.
[10] O.M. Andersen, C.-H. Yeung, H. Vorum, M. Wellner, T.K. Andreassen, B. Erdmann, E.-C. Mueller, J. Herz, A. Otto, T.G. Cooper, T.E. Willnow, Essential role of the apolipoprotein E receptor-2 in sperm development, J. Biol. Chem. 278 (2003) 23989–23995.
[11] G.E. Olson, V.P. Winfrey, S.K. NagDas, K.E. Hill, R.F. Burk, Apolipoprotein E receptor-2 (apoER2) mediates selenium uptake from selenoprotein P by the mouse testis, J. Biol. Chem. 282 (2007) 12290–12297.
[12] M.T.T. Pennings, R.H.W.M. Derksen, R.T. Urbanus, W.L. Tekelenburg, W. Hemrika, P. G. De Groot, Platelets express three different splice variants of apoER2 that are all involved in signaling, J. Thromb. Haemost. 5 (2007) 1538–1544.
[13] R.T. Urbanus, M.T.T. Pennings, R.H.W.M. Derksen, P.G. de Groot, Platelet activation by dimeric beta2-glycoprotein I requires signaling via both glycoprotein Ibalpha and apolipoprotien E receptor 2′, J. Thromb. Haemost. 6 (2008) 1405–1412.
[14] D.R. Riddell, D.V. Vinogradov, A.K. Stannard, N. Chadwick, J.S. Owen, Identification and characterization of LRP8 (apoER2) in human blood platelets, J. Lipid Res. 40 (1999) 1925–1930.
[15] I. Korschineck, S. Ziegler, J. Breuss, I. Lang, M. Lorenz, C. Kaun, P.F. Ambros, B.R. Binder, Identification of a novel exon in apolipoprotein E receptor 2 leading to alternatively spliced mRNAs found in cells of the vascular wall but not in neuronal tissue, J. Biol. Chem. 276 (2001) 13192–13197.
[16] S.M. Sacre, A.K. Stannard, J.S. Owen, Apolipoprotein E (apoE) isoforms differentially induce nitric oxide production in endothelial cells, FEBS Lett. 540 (2003) 181–187.
[17] S. Ramesh, C.N. Morrell, C. Tarango, G.D. Thomas, I.S. Yuhanna, G. Girardi, J. Herz, R.T. Urbanus, P.G. de Groot, P.E. Thorpe, J.E. Salmon, P.W. Shaul, C. Mineo, Antiphospholipid antibodies promote leukocyte–endothelial cell adhesion and thrombosis in mice by antagonizing eNOS via b2GPI and apoER2, J. Clin. Invest. 121 (2011) 120–131.
[18] X.V. Yang, Y. Banerjee, J.A. Fernandez, H. Deguchi, X. Xu, L.O. Mosnier, R.T. Urbanus, P.G. de Groot, T.C. White-Adams, O.J.T. McCarty, J.H. Griffin, Activated protein C ligation of apoER2 (LRP8) causes Dab1-dependent signaling in U937 cells, Proc. Natl. Acad. Sci. U. S. A. 106 (2009) 274–279.
[19] X. Chen, Z. Guo, E.U. Okoro, H. Zhang, L. Zhou, X. Lin, A.T. Rollins, H. Yang, Up-regulation of ATP binding cassette transporter A1 expression by very low density

lipoprotein receptor and apolipoprotein E receptor 2, J. Biol. Chem. 287 (2012) 3751–3759.
[20] D.R. Riddell, A. Graham, J.S. Owen, Apolipoprotein E inhibits platelet aggregation through the L-arginine:nitric oxide pathway, J. Biol. Chem. 272 (1997) 89–95.
[21] J.O. Robertson, W. Li, R.L. Silverstein, E.J. Topol, J.D. Smith, Deficiency of LRP8 in mice is associated with altered platelet function and prolonged time for in vivo thrombosis, Thromb. Res. 123 (2008) 644–652.
[22] A.K. Stannard, D.R. Riddell, S.M. Sacre, A.D. Tagalakis, C. Langer, A. von Eckardstein, P. Cullen, T. Athanasopoulos, G. Dickson, J.S. Owen, Cell-derived apolipoprotein E (ApoE) particles inhibit vascular cell adhesion molecule-1 (VCAM-1) expression in human endothelial cells, J. Biol. Chem. 276 (2001) 46011–46016.
[23] M.T. Pennings, R.H. Derksen, M. van Lummel, J. Adelmeijer, K. Vanhoorelbeke, R.T. Urbanus, T. Lisman, P.G. De Groot, Platelet adhesion to dimeric beta2-glycoprotein-1 under conditions of flow is mediated by at least two receptors: glycoprotein 1b-alpha and APOER2′, J. Thromb. Haemost. 5 (2007) 369–377.
[24] M.T. Pennings, M. van Lummel, R.H. Derksen, R.T. Urbanus, R.A. Romijn, P.J. Lenting, P.G. De Groot, Interaction of beta2 glycoprotein 1 with members of the low density lipoprotein receptor family, J. Thromb. Haemost. 4 (2006) 1680–1690.
[25] A. Kodvawala, A.B. Ghering, W.S. Davidson, D.Y. Hui, Carboxyl ester lipase expression in macrophages increases cholesteryl ester accumulation and promotes atherosclerosis, J. Biol. Chem. 280 (2005) 38592–38598.
[26] M.D. Puente Navazo, L. Daviet, E. Ninio, J.L. McGregor, Identification on human CD36 of a domain (155–183) implicated in binding oxidized low-density lipoproteins (Ox-LDL), Arterioscler. Thromb. Vasc. Biol. 16 (1996) 1033–1039.
[27] A. Daugherty, D.L. Rateri, Development of experimental designs for atherosclerosis studies in mice, Methods Cell Biol. 36 (2005) 129–138.
[28] J.B. Lingrel, R. Pilcher-Roberts, J.E. Basford, P. Manoharan, J. Neumann, E.S. Konaniah, R. Srinivasan, V.Y. Bogdanov, D.Y. Hui, Myeloid-specific Kruppel-like factor 2 inactivation increases macrophage and neutrophil adhesion and promotes atherosclerosis, Circ. Res. 110 (2012) 1294–1302.
[29] S.J. Hardwick, L. Hegyi, K. Clare, N.S. Law, K.L. Carpenter, M.J. Mitchinson, J.N. Skepper, Apoptosis in human monocyte-macrophages exposed to oxidized low density lipoprotein, J. Pathol. 179 (1996) 294–302.
[30] V.C. Reid, M.J. Mitchinson, Toxicity of oxidised low density lipoprotein towards mouse peritoneal macrophages in vitro, Atherosclerosis 98 (1993) 17–24.
[31] W. Li, H. Dalen, J.W. Eaton, X.-M. Yuan, Apoptotic death of inflammatory cells in human atheroma, Arterioscler. Thromb. Vasc. Biol. 21 (2001) 1124–1130.
[32] W. Li, L. Kornmark, L. Jonasson, C. Forssell, X.-M. Yuan, Cathepsin L is significantly associated with apoptosis and plaque destabilization in human atherosclerosis, Atherosclerosis 202 (2009) 92–102.
[33] D.F.D. Mahmood, I. Jguirim-Souissi, E.-H. Khadija, N. Blondeau, V. Diderot, S. Amrani, M.-N. Slimane, T. Syrovets, T. Simmet, M. Rouis, Peroxisome proliferator-activated receptor gamma induces apoptosis and inhibits autophagy of human monocyte-derived macrophages via induction of cathepsin L. Potential role in atherosclerosis, J. Biol. Chem. 286 (2011) 28858–28866.
[34] M.F. Lavin, N. Gueven, The complexity of p53 stabilization and activation, Cell Death Differ. 13 (2006) 941–950.
[35] G. Chinetti, S. Griglio, M. Antonucci, I.P. Torra, P. Delerive, Z. Majd, J.-C. Fruchart, J. Chapman, J. Najib, B. Staels, Activation of proliferator-activated receptors α and γ induces apoptosis of human monocyte-derived macrophages, J. Biol. Chem. 273 (1998) 25573–25580.
[36] T.-C. Ho, Y.-C. Yang, S.-L. Chen, P.-C. Kuo, H.-K. Sytwu, H.-C. Cheng, Y.-P. Tsao, Pigment epithelium-derived factor induces THP-1 macrophage apoptosis and necrosis by the induction of the peroxisome proliferator-activated receptor gamma, Mol. Immunol. 45 (2008) 898–909.
[37] I. Tabas, Consequences and therapeutic implications of macrophage apoptosis in atherosclerosis: the importance of lesion stage and phagocytic efficiency, Arterioscler. Thromb. Vasc. Biol. 25 (2005) 2255–2264.
[38] H. Li, J.J. Repa, M.A. Valasek, E.P. Beltroy, S.D. Turley, D.C. German, J.M. Dietschy, Molecular, anatomical, and biochemical events associated with neurodegeneration in mice with Niemann–Pick Type C disease, J. Neuropathol. Exp. Neurol. 64 (2005) 323–333.
[39] K. Kysenius, P. Muggalla, K. Matlik, U. Arumae, H.J. Huttunen, PCSK9 regulates neuronal apoptosis by adjusting apoER2 levels and signaling, Cell. Mol. Life Sci. 69 (2012) 1903–1916.
[40] C.-Y. Wu, Z.-H. Tang, L. Jiang, X.-F. Li, Z.-S. Jiang, L.-S. Liu, PCSK9 siRNA inhibits HUVEC apoptosis induced by ox-LDL via Bcl/Bax-caspase9-caspase3 pathway, Mol. Cell. Biochem. 359 (2012) 347–358.
[41] U. Beffert, G. Morfini, H.H. Bock, H. Reyna, S.T. Brady, J. Herz, Reelin-mediated signaling locally regulates protein kinase B/Akt and glycogen synthase kinase 3beta, J. Biol. Chem. 277 (2002) 49958–49964.
[42] P. Tontonoz, L. Nagy, J.G.A. Alvarez, V.A. Thomazy, R.M. Evans, PPAR-gamma promotes monocyte/macrophage differentiation and uptake of oxidized LDL, Cell 93 (1998) 241–252.
[43] M. Febbraio, D.P. Hajjar, R.L. Silverstein, CD36: a class scavenger receptor involved in angiogenesis, atherosclerosis, inflammation, and lipid metabolism, J. Clin. Invest. 108 (2001) 785–791.
[44] K.H. Han, M.K. Chang, A. Boullier, S.R. Green, A. Li, C.K. Glass, O. Quehenberger, Oxidized LDL reduces monocyte CCR2 expression through pathways involving peroxisome proliferator-activated receptor gamma, J. Clin. Invest. 106 (2000) 793–802.
[45] G. Chinetti, S. Lestavel, V. Bocher, A.T. Remaley, B. Neve, I.P. Torra, E. Teissier, A. Minnich, M. Jaye, N. Duverger, H.B.J. Brewer, J.-C. Fruchart, V. Clavey, B. Staels, PPAR-alpha and PPAR-gamma activators induce cholesterol removal from human macrophage foam cells through stimulation of the ABCA1 pathway, Nat. Med. 7 (2001) 53–58.
[46] A.C. Li, K.K. Brown, M.J. Silvestre, T.M. Willson, W. Palinski, C.K. Glass, Peroxisome proliferator-activated receptor gamma ligands inhibit development of atherosclerosis in LDL receptor-deficient mice, J. Clin. Invest. 106 (2000) 523–531.
[47] V.R. Babaev, R.P. Runner, D. Fan, L. Ding, Y. Zhang, H. Tao, E. Erbay, C.Z. Gorgun, S. Fazio, G.S. Hotamisligil, M.F. Linton, Macrophage Mal1 deficiency suppresses atherosclerosis in low density lipoprotein receptor-null mice by activating peroxisome proliferator-activated receptor-gamma regulated genes, Arterioscler. Thromb. Vasc. Biol. 31 (2011) 1283–1290.
[48] E. Thorp, G. Kuriakose, Y.M. Shah, F.J. Gonzalez, I. Tabas, Pioglitazone increases macrophage apoptosis and plaque necrosis in advanced atherosclerotic lesions of nondiabetic low-density lipoprotein receptor-null mice, Circulation 116 (2007) 2182–2190.
[49] S.E. Nissen, K. Wolski, Effect of rosiglitazone on the risk of myocardial infarction and death from cardiovascular causes, N. Engl. J. Med. 356 (2007) 2457–2471.
[50] P.D. Home, S.J. Pocock, H. Beck-Nielsen, R. Gomis, M. Hanefeld, N.P. Jones, M. Komajda, J.J. McMurray, Rosiglitazone evaluated for cardiovascular outcomes: an interim analysis, N. Engl. J. Med. 357 (2007) 28–38.
[51] L. Villacorta, F.J. Schopfer, J. Zhang, B.A. Freeman, Y.E. Chen, PPARgamma and its ligands: therapeutic implicat\ions in cardiovascular disease, Clin. Sci. (Lond.) 116 (2009) 205–218.